Pressure dependence of the *A-B* phase transition temperature in superfluid ^{3}He in 1.1-μm slab geometry

S. Miyawaki, K. Kawasaki, H. Inaba, A. Matsubara, O. Ishikawa, T. Hata, and T. Kodama*
Graduate School of Science, Osaka City University, Osaka 558-8585, Japan
(Received 22 February 2000)

To investigate the size effects of superfluid ^{3}He in a slab geometry, we made a sample cell which has very uniform 1.1 μm spacing by stacking 440 films, where the static magnetic field for NMR was fixed parallel to the film surface. We performed cw NMR experiments in the superfluid state and observed the jump of resonance frequency shift at 10, 20, 24, and 27 bar. We attributed these phenomena to the *A-B* phase transition which occurs in 1.1 μm slab spacing at the temperature $T_{AB}(1.1\ \mu\mathrm{m})$. The *A-B* phase transition temperatures were suppressed by about 15% from those of the bulk liquid at higher pressures. When we coated the film surface with some ^{4}He layers, we observed that the $T_{AB}(1.1\ \mu\mathrm{m})$ became higher with increasing surface ^{4}He layers.

I. INTRODUCTION

The anisotropy and the long coherence length of the superfluid ^{3}He play an important role on the phase diagram in a confined geometry. The superfluid ^{3}He is known as the **p**-wave BCS state, which allows theoretically various phases in the ordered state. Three different phases *A*, *B*, and *A*1 have been observed experimentally in bulk liquid. At zero external magnetic field, the *A* phase exists only in the high pressure region and the *B* phase is in the low pressure and low temperature region. When the external magnetic field is applied the polycritical point (PCP) disappears and the *A*1 phase appears in the very narrow region just below the transition temperature. These observed *A* and *B* phase have been recognized as the *ABM* and the *BW* state, respectively,[1,2] and can be described by using the complicated **p**-wave order parameter. The *ABM* state is the anisotropic state which has the axial symmetry and the *BW* state is the isotropic state.

Ginzburg and Landau[3] introduced a phenomenological order parameter *A* which had the meaning that $|A|^2$ represented the local density of superconducting electrons or superfluid component defined in the two-fluid model. They expanded the free energy difference between the ordered state and the normal state in power of $|A|^2$ and $|\nabla A|^2$, where the gradient terms were introduced to take account of the spatial variation of *A*. For the **s**-wave BCS state, this free energy difference δF is written by

$$\delta F = -\alpha|A|^2+\beta|A|^4+K|\nabla A|^2, \tag{1}$$

where the temperature dependence of α is given by $\alpha(T)=\alpha_0(1-T/T_c)$ and α_0, β, and K are the positive constants near the transition temperature T_c. Provided that the slow spatial variation of the order parameter, a characteristic length can be defined by $\xi(T)=\sqrt{K/\alpha}=\xi(0)(1-T/T_c)^{-1/2}$ from Eq. (1). This length is related to the **s**-wave BCS coherence length ξ_s by $\xi(0)=\sqrt{3/5}\xi_s$.[4] ξ_s is given by

$$\xi_s=\sqrt{\frac{7\zeta(3)}{48}}\frac{\hbar v_F}{\pi k_B T_c}, \tag{2}$$

where $\zeta(3)$ is Riemann's zeta function, k_B is the Boltzmann constant and v_F is the Fermi velocity.

The Ginzburg and Landau (GL) expansion of the free energy difference was applied to the **p**-wave superfluid state in terms of complex 3×3 matrix by Mermin and Stare.[5] Ambegaokar, de Gennes, and Rainer (AGR) studied the spatial variation of order parameter and the boundary conditions at a smooth and a rough surfaces in the superfluid ^{3}He.[6] By considering how ^{3}He quasiparticles collide with the surface the order parameter can be separated into the longitudinal and the transverse components governed by the different coherence lengths ξ_L and ξ_T, respectively, $\xi_L=\sqrt{3}\xi(T)$, $\xi_T=\xi(T)$ in the weak coupling approximation. In the vicinity of specular surfaces the transverse component does not change, but the longitudinal component becomes small and vanishes at the surface due to the pair breaking. Since the surface suppresses the longitudinal component of the order parameter, the *BW* state, which has an isotropic energy gap, will loose the condensation energy near the container wall. On the other hand, the anisotropic superfluid states, such as the planar state or the *ABM* state, are expected to keep their condensation energy near the surface. Actually the *ABM* state can exist without any energy loss by anchoring its ***l*** vector, the angular momentum of **p**-wave pair, perpendicular to the surface. The transverse component is also suppressed though by different amounts when quasiparticles diffusively scatter at the rough surface.

The theoretical calculations for various geometries based on the AGR theory and on the GL expansion have been carried out by many authors to discuss the stability of the superfluid ^{3}He state. Barton and Moore[7] predicted the stability of two additional phase in the cylindrical pore, and Privorotskii[8] found that the walls stabilized the *ABM* state in the vicinity of the PCP. Fujita *et al.*[10] showed that in the thin film whose thickness was smaller than about ten times of $\xi(T)$ the planar state or the *ABM* state became stable instead of the *BW* state. A numerical calculation for the superfluid transition temperature with a rough surface has been performed by Kjäldman *et al.*[9] for cylindrical and thin film geometries. They expected that there should be a clear suppres-

sion of transition temperature in the cell whose characteristic size was less than ten times of the coherence length $\xi(0)$ and that no superfluidity might occur if the cell size was comparable to $\xi(0)$.

Recently, more systematic calculations for the superfluid ^{3}He in these restricted geometries have been performed. Hara and Nagai[11] studied in the weak coupling limit the *A*-*B* phase transition of superfluid ^{3}He in a slab geometry with specular walls. They derived the critical thickness of ^{3}He film where the *B* phase (*BW* state) became unstable. Above the temperature at which the spacing of the slab geometry is about eight times of $\xi(T)$ the *A* phase (*ABM* state) is expected to become stable instead of the *B* phase. Fetter and Ullah[12] and Li and Ho[13] presented the phase diagrams of superfluid ^{3}He in some sizes of narrow slab geometry and thin cylinder. They showed that the *A* phase became more stable at a lower pressure when the size became smaller and also pointed out the mechanism of boundary scattering of ^{3}He quasiparticles was crucial to determine the phase diagram. The specular scattering will favor the *A* phase at low temperature and at low pressure more than the diffusive scattering because the anisotropic *A* phase has an advantage of the condensation energy in such a condition.

Several experiments have been performed to study how ^{3}He quasiparticles are scattered at the surface by measuring the transition temperature and the critical current in narrow channels[14,15] and in saturated films,[16,17] and the superfluid density in porous materials.[18] In these measurements, it was found that quasiparticles have been usually scattered diffusively at the container surface. Recently, it has become clear that the diffusive boundary conditions of ^{3}He quasiparticles can be altered to the specular one by the adsorbed ^{4}He atoms on the surface of porous media in the fourth sound experiment,[19] and in the torsional oscillator experiments,[20,21] and of combined NMR and torsional oscillator experiment.[22] Such a change of scattering mechanism seems to be related to the superfluidity of ^{4}He film but the microscopic mechanism is not clear.

The experimental work in the thin slab geometry using NMR method have been performed by some groups. Ahonen *et al.*[23] performed cw NMR experiments in the 4 μm slab, and they observed a reduction in the $B \rightarrow A$ transition temperature, a negative cw NMR shift in the *A* phase which was caused by a textual anisotropy. The superfluid ^{3}He confined in 0.3 μm slab spacing was investigated by Freeman *et al.*[22] using pulsed NMR and torsional oscillator method. They studied at low enough temperatures where the *A*-*B* phase transition was expected to occur in this size but only the *A* phase was observed. Their result was thought to be attributed to the supercooling phenomena because the *A*-*B* transition is the first order phase transition. Recently Kawae *et al.*[24] reported the observation of the *A*-*B* transition in a thin slab geometry, but their cell had a wide distribution of spacing between plates and both phase signals coexisted.

So far there is no measurement which shows a clear phase transition between the superfluid phases in superfluid ^{3}He in a confined geometry which has a well defined size. To investigate this subject, the uniformity of sample spacing is very important. We, therefore, made the slab geometry which has a fairly uniform 1.1 μm spacing by stacking thick films, and performed cw and pulsed NMR experiments to study the phase transition in the superfluid state in the slab geometry.

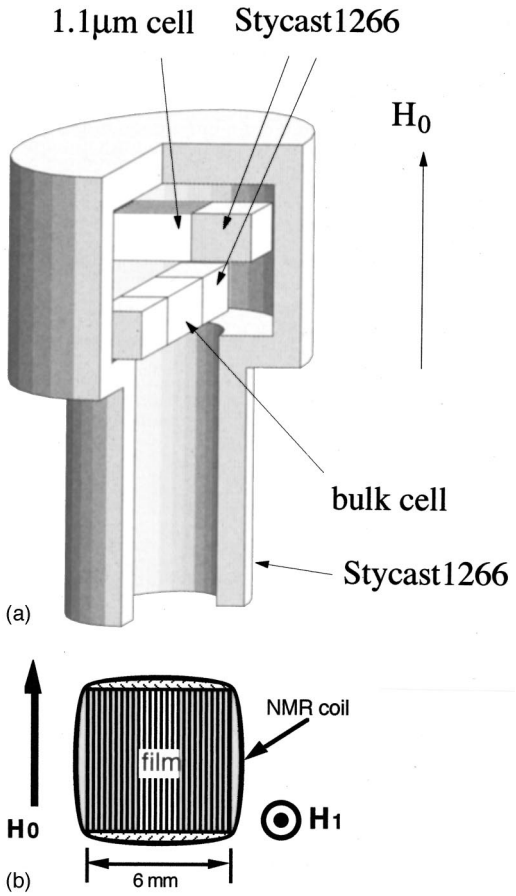

FIG. 1. (a) The close view of 1.1 μm cell and bulk cell. To avoid the mutual interaction of H_1 coil, two H_1 coils are arranged with a right angle to each other. (b) The cross sectional view of film stack.

This paper is organized as follows. In Sec. II we describe the experimental details. In Sec. III A we discuss the overall behavior of cw NMR signals. In Sec. III B we show results of superfluid ^{3}He in 1.1-μm slab geometry and discuss the identification of superfluid phase. In Sec. III C we show the phase diagram and the supercooling phenomena. Finally we summarize our results.

II. EXPERIMENTAL

Our experiments were performed using a copper nuclear demagnetization cryostat. The sample cell we have used is illustrated in Fig. 1. The slab geometry was made by stacking 440 polyethylene films, Lumirror,[25] on which uniform beads of 1.1 μm diameter, Uniform Latex Particle,[26] were sparsely populated in the mean distance 30 μm to establish the spacing. This film surface was sufficiently flat and clean. These latex beads were deposited on the film surface by misting a suspension of micro spheres in isopropanol onto the film and allowing the alcohol to evaporate. This method of achieving a spacing with latex spheres was used previously by Freeman and Richardson.[22] Although it is needed to use films as thin as possible to have a large filling fraction of liquid ^{3}He in the NMR coil, we have selected a bit thick film

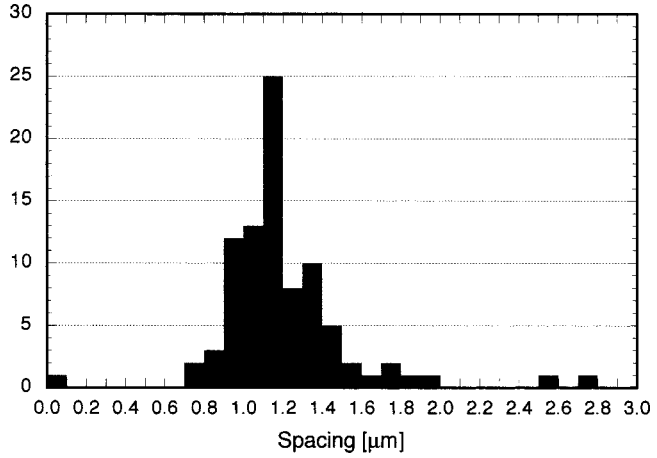

FIG. 2. The distribution of slab spacing. The spacing is measured with EPMA, after cutting the film stack at arbitrary section.

of 12 μm thickness, because the sufficient hardness of the film is required to keep the slab spacing uniform. The cw NMR signal, however, has enough intensity to be detected. Figure 2 shows the distribution of spacing obtained by the electron probe microanalyzer (EPMA). From this direct observation, we can check the uniformity of our sample cell and find that the mean sheet spacing is $1.12 \pm 0.04\ \mu$m. We call this cell as 1.1 μm cell below.

These stacked films was packed tightly into a Stycast 1266 epoxy holder, and the NMR coil was directly wound around this holder [Fig. 1(b)]. In addition, to compare the signal from 1.1 μm cell with that from bulk liquid, we also prepared the bulk liquid cell which was made by hollowing out a Stycast block, and the NMR coil was wound in the same way as the 1.1 μm cell. These two sample cells were put in the experimental apparatus which was thermally anchored to the nuclear stage as shown in Fig. 3. The temperature of liquid ^{3}He was measured by pulsed NMR thermometer of Pt wire with a sintered silver heat exchanger immersed in liquid ^{3}He. The Curie susceptibility of this Pt wire was calibrated against the ^{3}He melting curve thermometer in the few mK region.[27]

To achieve the homogeneous static magnetic field for

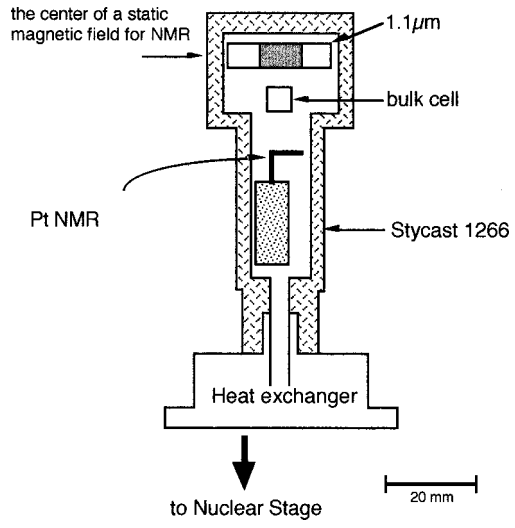

FIG. 3. The schematic diagram of experimental apparatus.

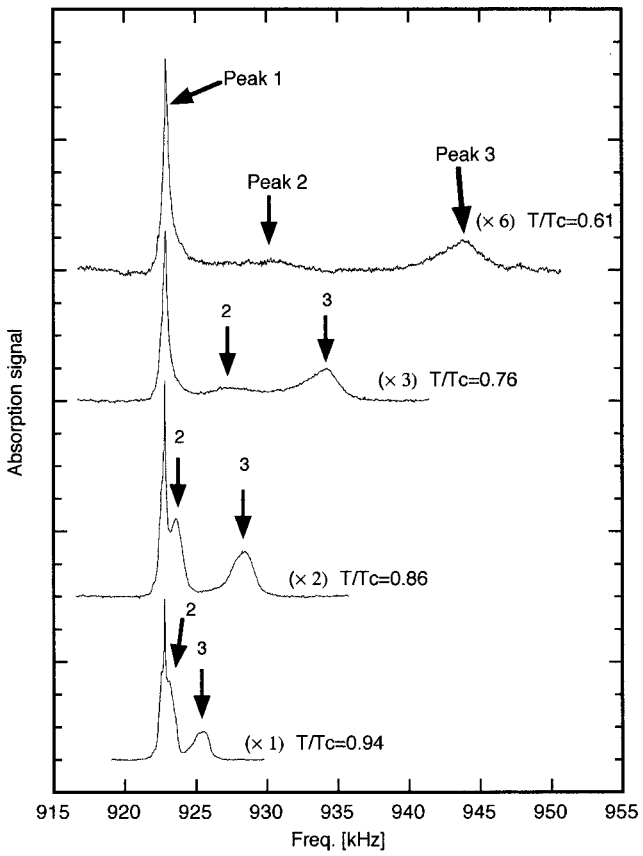

FIG. 4. The cw NMR spectra of pure liquid ^{3}He at 24 bar. Three different peaks observed at each cw NMR spectrum are labeled as peak 1, peak 2, and peak 3, respectively. Since the signal intensity extremely depends on the temperature, it is adjusted by multiplying some coefficients as shown.

NMR measurements, we made the solenoid magnet using the single filament superconducting wire (Nb-Ti with Cu clad) which was wound on the radiation shield of the mixing chamber. This magnet had 98 mm diameter and 217 mm length and also had two kinds of compensation magnets which were used for the first order and the second order correction. These NMR magnet sets helped us to have a high homogeneity of 10^{-4} at two ^{3}He NMR cells and at Pt NMR cell simultaneously. The direction of H_0 field for NMR is fixed parallel to the film surfaces. We have mainly performed cw NMR and sometimes pulsed NMR to recognize the superfluid phase. In cw NMR measurement the magnetic field was swept with the fixed NMR operating frequency of 922.5 kHz. All the data were obtained on warming up from the lowest temperature except those at 10 bar with adsorbed ^{4}He atom.

III. RESULTS

A. Identification of cw NMR spectrum

A several cw NMR spectra of pure superfluid ^{3}He obtained from 1.1 μm cell at 24 bar are shown in Fig. 4 in temperatures below $T = 0.94 T_c$, where only the *B* phase signals are observed in the bulk liquid cell. In this paper, we use the reduced temperatures which are normalized by the transition temperature T_c of bulk liquid. From Fig. 4, we can find that our raw cw NMR spectrum is composed of three differ-

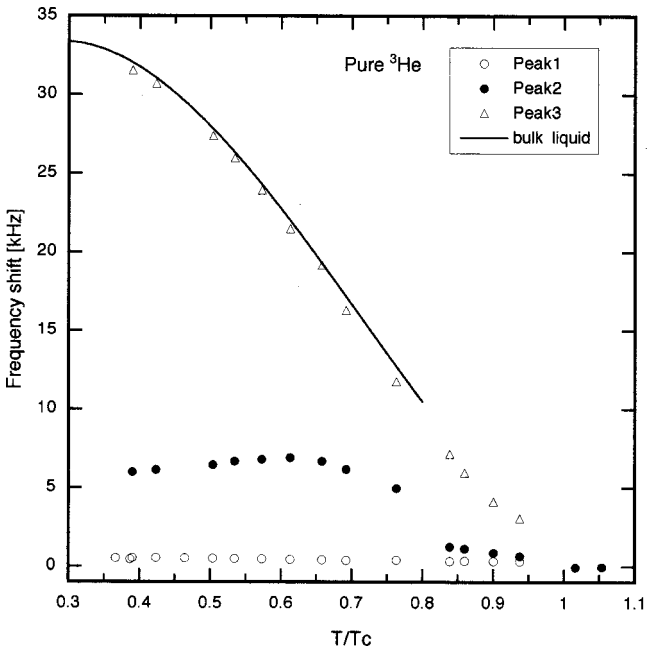

FIG. 5. The temperature dependence of frequency shift for peak 1, peak 2, and peak 3 at 24 bar in pure liquid ^{3}He; open circles for peak 1, solid circles for peak 2, open triangles for peak 3. Solid curve is calculated with the longitudinal frequency of bulk liquid *B* phase.

ent peaks. We label these peaks from the lower frequency side peak 1, peak 2, and peak 3, respectively. For peak 1 both the resonance frequency and the line width are independent of temperature but they are strongly dependent on temperature for peak 2 and peak 3. The resonance frequencies of these peaks are plotted in Fig. 5 in the form of the frequency shift from the resonance frequency just above T_c. The peak 3 signals are shifted continuously toward the higher frequency side with decreasing temperatures. On the other hand, the peak 2 signals have the jump of frequency shift at around $T=0.8T_c$ and there is a maximum of frequency shift at $T=0.6T_c$. Above $T=0.94T_c$, three peaks are so close to each other that we cannot distinguish them at all. At other pressures we always observed three peaks, which had the similar temperature dependence to those at 24 bar.

To know what these signals are, we first consider the detail structures inside the NMR coil. There is a possibility to exist some extra volume around the stacked films as shown in Fig. 1(b), in the upper and lower space and also in the side space, because we did not glue up the pick up coil just around the holder completely. So the raw NMR spectrum might include signals coming from these extra volume. When we applied the magnetic field gradient parallel to the static magnetic field, only the peak 1 signal was split into two peaks whose splitting frequency corresponds with the frequency difference between the positions about 6 mm apart from each other along the field gradient. This 6 mm is just the holder size in Fig. 1(b), on which the NMR coil is wounded. This behavior was independent of temperature. This result strongly indicates that the peak 1 signal is coming from the liquid in the upper and lower space outside films in the NMR coil.

Next we compare the peak 3 frequency with the frequency shift of bulk superfluid ^{3}He in the *B* phase where the magnetic field and the **n** vector, the rotation axis in the order parameter, show the non-Leggett configuration. In this configuration the resonance frequency ν in cw NMR experiments is determined by the angle θ between the **n** vector and the magnetic field in the form $\nu^2=\nu_L^2+\sin^2\theta\times(\nu_L^B)^2$, where ν_L is the Larmor frequency and ν_L^B is the longitudinal resonance frequency of the bulk *B* phase. The angle θ is determined by the combination of the dipole energy, the magnetic field energy, and the pair breaking effect at the surface.[28] This relation has been confirmed experimentally by Ahonen *et al.*[23] By using the data of ν_L^B of Ahonen *et al.* it is found that our peak 3 frequency shifts are well fitted by the above equation at all temperatures and also at all pressures when $\sin^2\theta$ is 0.8 in Fig. 5. It was confirmed experimentally that the surface magnetic field energy is minimized with $\sin^2\theta=0.8$ by Ahonen *et al.* and Ishikawa *et al.*,[29] when the magnetic field is applied parallel to the surface. This means that the peak 3 signal is attributed to the *B* phase which exists close to the surface and that the static magnetic field is parallel to the surface. The fact that the longitudinal resonance frequency of bulk liquid explained peak 3 well with $\sin^2\theta=0.8$ means the size of liquid is much larger than the coherence length but is smaller than the healing length of the **n** vector to have the uniform **n** texture. The only corresponding position in our cell is the side space around the stacked films in the NMR coil.

In Sec. III B, we will discuss the magnetization of each peak in the superfluid state and the effect of ^{4}He surface layer. It will be clear that the magnetization of peak 1 and peak 3 will decrease with decreasing temperature below $T=0.95T_c$ at 24 bar and become constant at sufficiently low temperature. When we put ^{4}He layer on the surface, only the peak 2 signal was changed but the signals of peak 1 and peak 3 were not affected by any ^{4}He coverage (see below). These results also support peak 1 and peak 3 had the *B* phase behavior in bulk liquid.

We conclude that peak 1 is the signal coming from the bulk liquid which is in the upper and lower space around the stacked films and that the *B* phase in this liquid is in the Leggett configuration where $\sin\theta=0$. In such a configuration the intrinsic relaxation mechanism of Leggett-Takagi relaxation is not operative and the dipole torque also is not operative in cw NMR measurement. Both no change of line width and no change of resonance frequency of peak 1 are consistent with the *B* phase behavior in the Leggett configuration. On the other hand, we conclude that peak 3 is the signal coming from the bulk liquid which is in the side space of the stacked films. The surface magnetic energy takes this liquid to the non-Leggett configuration in the *B* phase in which the Leggett-Takagi relaxation mechanism is operative and the line width becomes large in the uniform spin motion with decreasing temperature.[29] The observed changes of the line width of peak 3 is consistent with this behavior. We therefore conclude that only peak 2 is the signal coming from 1.1 μm slab spacing. We shall discuss about peak 2 as the signal in the 1.1 μm spacing in the following sections.

B. Superfluid ^{3}He

1. Pure ^{3}He

First we show the temperature dependence of peak 2 resonance frequency shift Δf below T_c at 10, 20, 24, and 27 bar

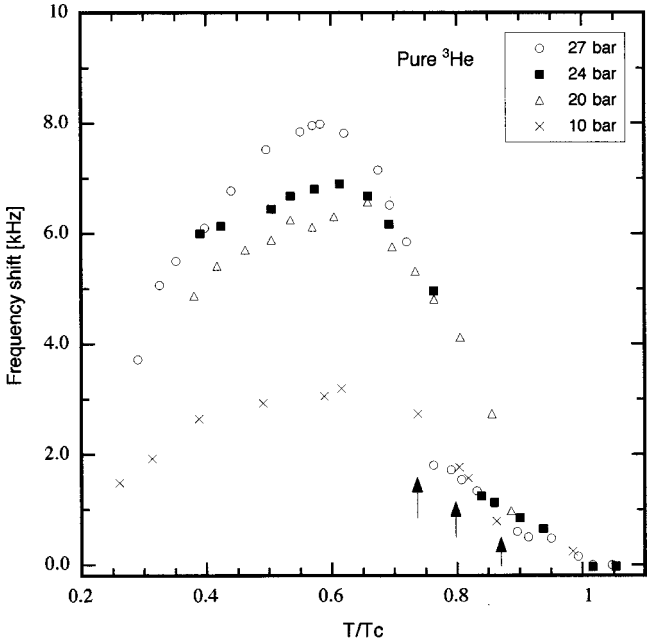

FIG. 6. The temperature dependence of peak 2 resonance frequency shift in pure liquid ^{3}He at 10, 20, 24, and 27 bar; crosses at 10 bar, open triangles at 20 bar, solid rectangulars for 24 bar, open circles for 27 bar.

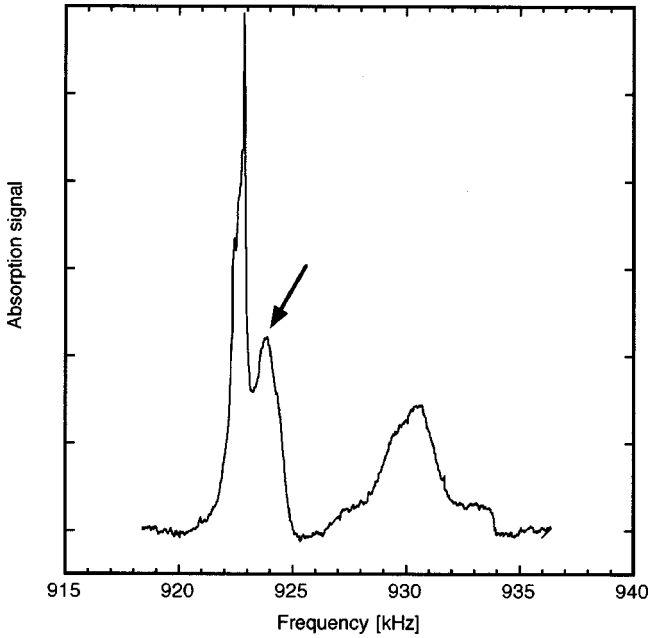

FIG. 7. The raw cw NMR spectrum at $T=0.82T_c$ at 27 bar. The magnetic field is fixed to have a resonance on peak 2 indicated by the arrow.

in Fig. 6. As mentioned in the previous section, we can see a jump of frequency shift at a particular temperature at each pressure. These jumps are indicated by arrows. At 10 and 20 bar they occurred nearly at the same reduced temperature. The jump in 10 bar is, however, not seen clearly in this scale. Another interesting point in Fig. 6 is that there exists a maximum of frequency shift at around $T=0.6T_c$ for each pressure, which is a considerably different behavior from that of the bulk liquid. All data in Fig. 6 were obtained on warming up process. Just above and below the frequency jump temperature, we always observed the only one resonance peak. Considering two peaks did not coexist at the same time, we think these jumps correspond to the phase transition in the superfluid state. Although the jump temperatures are lower than the *A-B* phase transition temperature in bulk liquid T_{AB} (bulk), it is likely that the high-temperature phase above the frequency jump temperature would be the *A* phase, because the *A* phase in bulk liquid exists at the high pressure and near T_c.

To check this conjecture, we performed the pulsed NMR experiments on the peak 2. We used the rf pulse with 200 μs of pulse width and set the magnetic field to have the resonance on peak 2 as shown by the arrow in Fig. 7. The data were stored in a computer after mixing the free induction decay FID signal with the local frequency with a frequency difference of 10 kHz from the NMR operating frequency and passing them through the low pass filter. The frequency spectra was obtained by FFT calculation. These spectra always consisted of a few peaks and we could separate the peak 2 spectrum from others by chasing it from a small tipping pulse. In Fig. 8, the frequency of peak 2 FID signal is plotted as a function of tipping angle β at 27 bar at $T=0.82T_c$, just above the frequency jump temperature but below T_{AB} (bulk). The solid curve is the characteristic curve of the tipping angle dependent frequency shift in the bulk *A* phase[30]

$$\frac{\Delta f(\beta)}{\Delta f(0)}=\frac{1}{4}(1+3\cos\beta). \tag{3}$$

All data agree very well with the theoretical curve of the bulk *A* phase. Data in pulsed NMR experiments at 10 and 24 bar also agree with Eq. (3). These results confirm that the high-temperature phase at each pressure is the *A* phase in the configuration where the ***l*** vector and the **d** vector are parallel

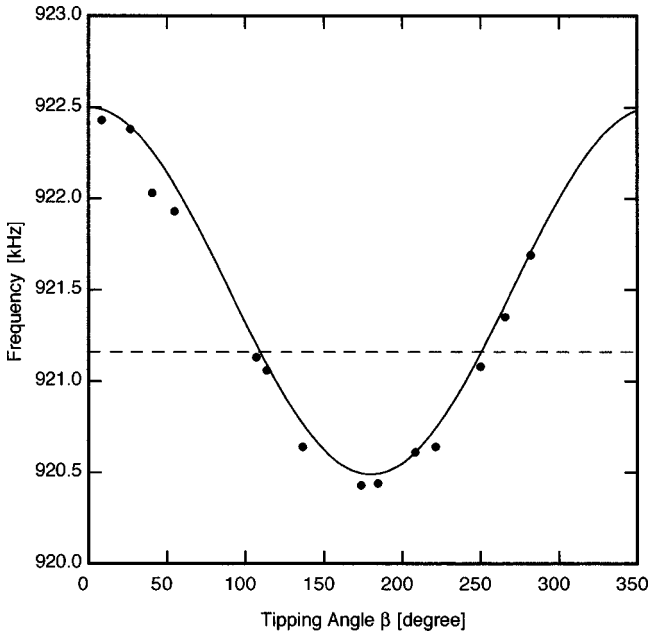

FIG. 8. The FID frequency vs tipping angle β at 27 bar. The solid line shows the calculated curve by using Eq. (3). The dashed line is the Larmor frequency in this experiment (921.16 kHz).

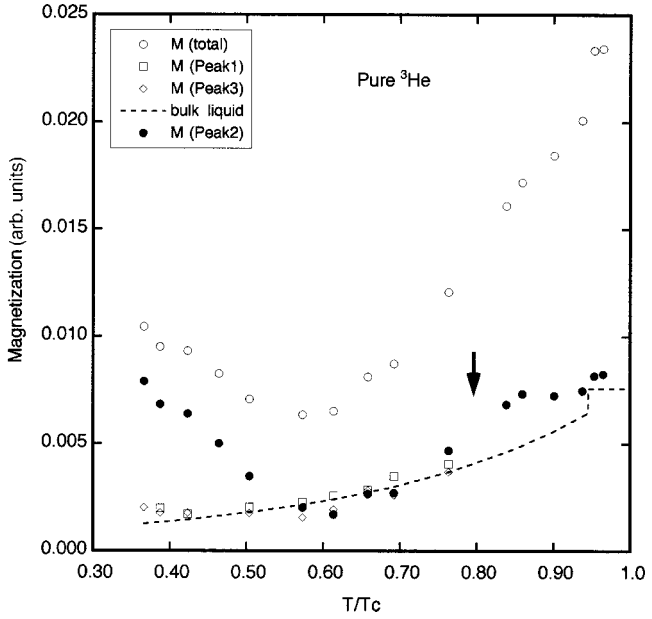

FIG. 9. The magnetization evaluated from cw NMR spectra at 24 bar in pure liquid ^{3}He; open circles for total magnetization, open rectangulars for peak 1, open diamonds for peak 3, solid circles for peak 2. The dashed line shows the temperature dependence of peak 1 and peak 3. The arrow indicates the temperature where the jump of frequency shift is observed. (See text for details.)

or antiparallel to each other in the equilibrium state, which is called the dipole locked state. Such a configuration of the ***l*** vector and the **d** vector is consistent with the expected one for the *A* phase in our cell, because both the dipole interaction energy and the magnetic field energy are minimized simultaneously in the dipole locked state with anchoring the ***l*** vector normal to the film surface. We tried to study the spin dynamics of the low-temperature phase of peak 2. However, it was impossible to get enough information from the FID signal because of less intensity of FID. We cannot see a clear difference in the frequency shifts between several pressures in the high-temperature phase because of scattered data.

Next we consider the magnetization. By using a Gaussian fitting curve on each peak, we integrated it numerically to obtain the quantities of magnetization and plotted them as a function of temperature at 24 bar in Fig. 9, where the peak 2 magnetization M (peak 2) was calculated by subtracting peak 1 and peak 3 magnetization from the total magnetization M (total), which was calculated by integrating the raw cw NMR spectra. At low enough temperatures, we could separate each peak and easily integrate peak 1 and peak 3 to get M (peak 1) and M (peak 3), respectively. We, however, could not manage to do the same manner near T_c, because all peaks were close to each other. As mentioned in the previous section, peak 1 and peak 3 are signals coming from the bulk liquid. By using the measured temperature dependence of magnetization in our bulk cell, we could extrapolate M (peak 1) and M (peak 3) toward T_c as long as peak 1 and peak 3 had the same transition temperature as T_{AB} (bulk). The characteristic features in Fig. 9 are as follows.

(a) The total magnetization decreases below T_c but has a minimum around $T=0.6T_c$ and increases at lower temperatures.

(b) The magnetization of peak 2 M (peak 2) is almost constant just below T_c and decreases below $T=0.8T_c$, but it has a minimum similar to the total magnetization at the same temperature and increases below $T=0.6T_c$.

The low temperature feature in (a) cannot be explained by the argument in the superfluid state because any pairing state does not show the gradual increase of the magnetic susceptibility with decreasing temperature. This point will be discussed in the next section. The (b) feature indicates that the magnetization M (peak 2) is responsible for the local minimum in M (total). The temperature where the M (peak 2) becomes small corresponds to the temperature where the jump of frequency shift is observed. The nearly constant magnetization M (peak 2) above this temperature is consistent with the *A* phase property. If a textural transition in one superfluid phase occurs, the NMR resonance frequency will change probably, but the susceptibility of the superfluid phase does not change suddenly in one phase. So the decrease of magnetization together with the jump of NMR resonance frequency indicates that a phase transition in the superfluid state occurred in the 1.1 μm cell at about $T=0.8T_c$ at 24 bar. At other pressures the same behavior of the magnetization of peak 2 is derived and the temperature of the onset of magnetization decrease also corresponds with the frequency jump temperature. With the result of pulsed NMR and the magnetization behavior, we confirm that the high-temperature phase in the 1.1 μm cell is the *A* phase. The decrease of the magnetization strongly suggests the low-temperature phase of peak 2 is the *B* phase.

2. Effect of surface ^{4}He

It is well known that the first and the second adsorbed layers on the cell surface are the solid ^{3}He in a high density state and these solids show the nearly paramagnetic and the ferromagnetic behavior, respectively.[31,32] The surface solid in pure ^{3}He liquid showed the ferromagnetic feature at low temperature as a whole.[22,24] Such a solid layer couples ^{3}He nuclear spin in liquid by a rapid atomic exchange which makes an average of the NMR frequency of solid and that of liquid with the help of a fast spin diffusion process in a narrow cell.[22] This averaging must occur in our cell because 1.1 μm is narrow enough that the fast spin diffusion process is expected. The measured frequency in such a combined system can be represented in the form

$$f_{\mathrm{meas}}=\frac{M_S}{M_S+M_L}f_S+\frac{M_L}{M_S+M_L}f_L, \tag{4}$$

where M_L and M_S are the magnetization of liquid and solid, and f_L and f_S are the resonance frequency of liquid and solid, respectively.[33]

We covered the surface of polyethylene film with a thin ^{4}He film to study how the polarized surface solid ^{3}He affected the entire signal of peak 2. Because of the preferential adsorption of the ^{4}He atom on the surface instead of the light ^{3}He atom, we expected the paramagnetic and ferromagnetic solid would disappear. In Fig. 10, we show the effect of the surface ^{4}He layer on the peak 2 resonance frequency at 24 bar. We used the surface density of 18, 13 μM/m^2 for the first layer, more than second layers, respectively.[22] With 1.5 ^{4}He layers on the film surface, the frequency shift Δf

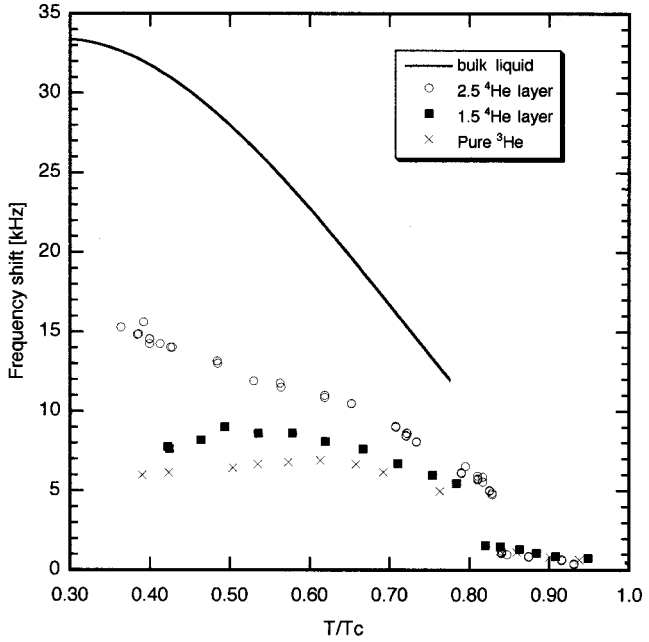

FIG. 10. The frequency shift of peak 2 for the different surface conditions at 24 bar; crosses for pure ^{3}He, solid rectangulars on adding 1.5 ^{4}He layer, open circles on adding 2.5 ^{4}He layer. The solid curve is calculated with the longitudinal frequency of bulk liquid *B* phase.

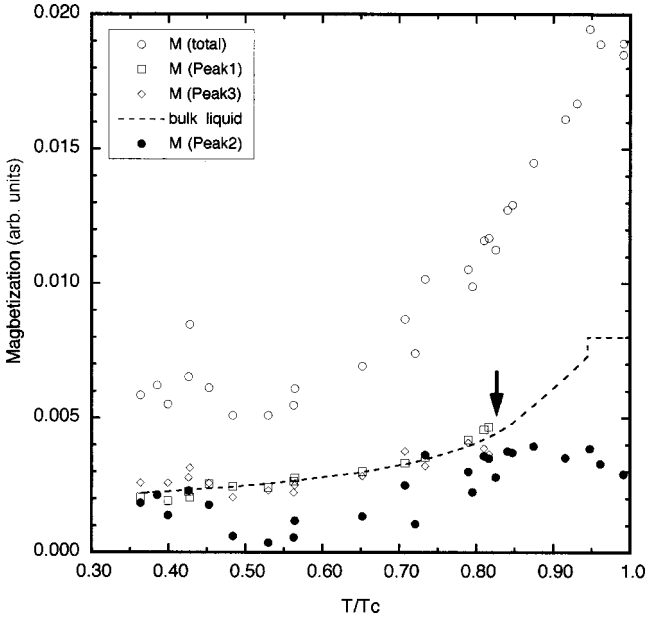

FIG. 11. The magnetization evaluated from cw NMR spectra at 24 bar with 2.5 ^{4}He layers; open circle for total magnetization, open rectangular for peak 1, open diamond for peak 3, solid circle for peak 2. The dashed line shows the temperature dependence of peak 1 and peak 3. The arrow indicates the temperature where the jump of frequency shift is observed. (See text for details)

became larger than that of pure ^{3}He and the temperature where the maximum frequency shift occurred decreased a bit. The Δf with 2.5 ^{4}He layers became more larger and increased monotonically with decreasing temperature down to $T=0.35T_c$ and the local maximum of the frequency shift disappeared. From Fig. 10, it is found that the surface solid affects largely the NMR behavior in pure ^{3}He in 1.1 μm films and the anomalous frequency behavior almost disappears by 2.5 ^{4}He layers. Figure 11 shows the magnetization M (peak 2) with 2.5 ^{4}He layers as a function of temperature, which is obtained by the same procedure as in Fig. 9. We can see the gradual decrease of M (peak 2) in the low-temperature phase with a small increase at the lowest temperature and also find M (peak 2) is constant in the high-temperature phase.

These results clearly show that the increase of M (peak 2) in pure ^{3}He at low temperature is due to the solid ^{3}He layer. We can understand the anomalous frequency behavior by using Eq. (4) as follows. The large solid magnetization makes $f_{\rm meas}$ close to the resonance frequency of solid which is almost the Larmor frequency, but the preferential adsorption of ^{4}He atom of 2.5 ^{4}He layers prohibits ^{3}He atom from making solid layers in the ferromagnetic state and M_S becomes small enough that $f_{\rm meas}$ becomes the resonance frequency of liquid which is positively shifted by the dipole torque in the superfluid state (see below). We think the frequency shift with 2.5 ^{4}He layers is almost due to the liquid itself except at lower temperatures.

Because the magnetization in the low-temperature phase in 1.1 μm cell behaves as the *B* phase without the surface solid ^{3}He, we conclude that the low-temperature phase is the *B* phase. We, therefore, confirm the phase transition in 1.1 μm cell in the superfluid state occurred with the frequency jump and the magnetization change, and also recognize the high-temperature phase is the *A* phase and the low-temperature phase is the *B* phase from the NMR properties. We call this phase transition temperature $T_{AB}(1.1\,\mu\text{m})$.

The positive frequency shift in 1.1 μm cell below $T_{AB}(1.1\,\mu\text{m})$ may be explained by the non-Leggett configuration in the *B* phase, which gives the frequency shift depending on the angle θ between the **n** vector and the magnetic field. The surface magnetic energy makes the non-Leggett configuration with the positive frequency shift in cw NMR, which has already been explained in the previous section. In Fig. 10 we also plotted the calculated NMR frequency shift in bulk liquid in the non-Leggett configuration with $\sin^2\theta=0.8$. The shift with 2.5 ^{4}He layers is nearly the half of the bulk shift but the temperature dependence is almost the same as the bulk shift. This means that the order parameter of the *B* phase is largely suppressed in the 1.1 μm cell, which is qualitatively consistent with the prediction using the pair breaking effect in *B* phase in a slab space.[6]

Here we comment about the magnetic field caused by the polarization. A ^{3}He spin in the solid layer feels the additional magnetic field from polarized ^{3}He dipoles in the solid layer itself. We observed the positive frequency shift of about 100 Hz near T_c in the normal state in comparison with the resonance frequency with 2.5 ^{4}He layers. This is the opposite result of Freeman *et al.*, where they observed the negative frequency shift for the small tipping pulse.[22] In our cell the surrounding ^{3}He dipoles make the internal magnetic field parallel to their polarization at a ^{3}He spin in the solid layer because the external field is parallel to the solid layer. Such a internal magnetic field is antiparallel to the polarization in the experiment of Freeman *et al.* in the equilibrium state since the external magnetic field is perpendicular to the solid layer. So the polarization in the solid layer in our cell will make the resonance frequency of solid changed from the

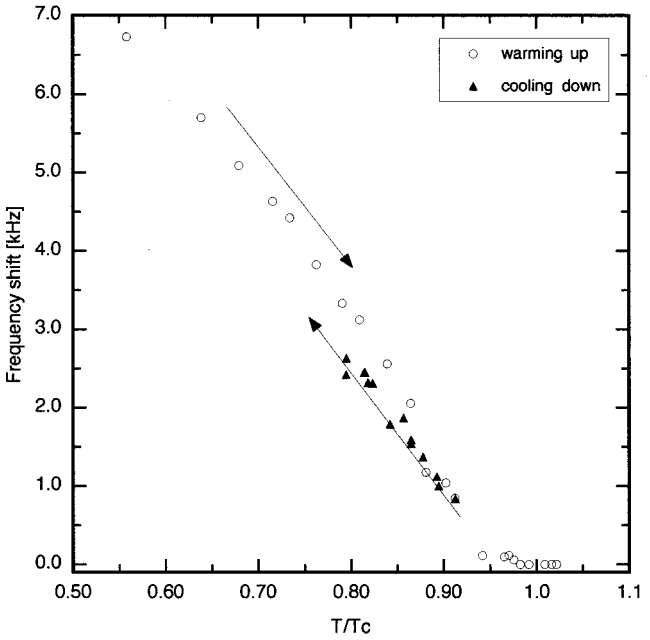

FIG. 12. The frequency shift of peak 2 with 2.5 ^{4}He layers at 10 bar. Open circles are data obtained during warming up and solid triangles are during cooling down. Data taken during cooling down show the supercooling. The solid line with arrow is a guide for the eye.

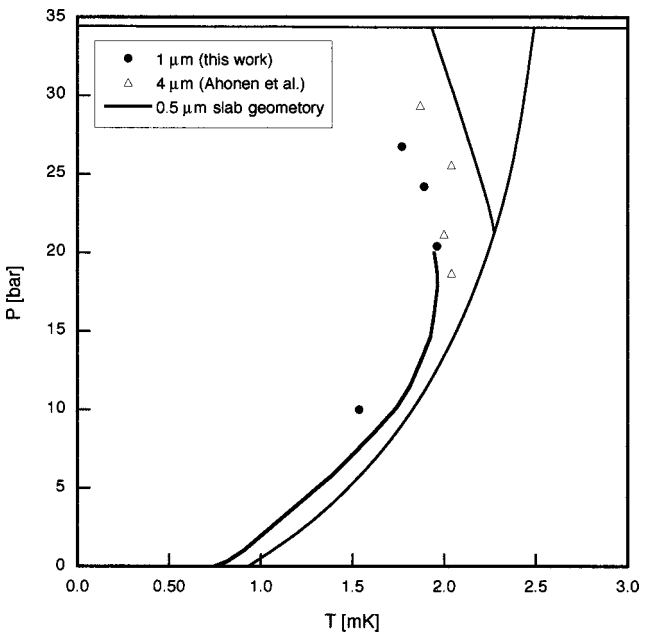

FIG. 13. The phase transition of pure liquid ^{3}He in 1.1 μm slab space. The solid circles are our results. The open triangles show the *A-B* phase transition in 4 μm slab space measured by Ahonen *et al.* The bold line is the theoretical calculation of *A-B* transition by Li and Ho (Ref. 13) for the 0.5 μm slab geometry with the diffusive scattering condition.

Larmor frequency a bit higher. This is responsible for the small positive shift of the resonance frequency of combined system in the 1.1 μm cell. However, we cannot obtain this quantity in the superfluid state clearly. The polarization of proton in Mylar sheets used by Freeman *et al.* had a large magnetic effect on ^{3}He spins but we observed no such a magnetic effect in the resonance frequency. We think the different material used in sheets is responsible for this difference.

We can roughly estimate the ratio of the frequency shift of Δf_A in the dipole locked *A* phase to Δf_B in non-Leggett configuration with $\sin^2\theta=0.8$ at the *A-B* phase transition by using the bulk liquid formula

$$\frac{\Delta f_A}{\Delta f_B}=\frac{1}{\sin^2\theta}\left(\frac{\nu_L^A}{\nu_L^B}\right)^2, \tag{5}$$

$$\left(\frac{\nu_L^A}{\nu_L^B}\right)^2=\frac{4}{15}\frac{\chi_B}{\chi_A}\left(\frac{\Delta_0^A}{\Delta_0^B}\right)^2=\frac{2}{15}\frac{\chi_B}{\chi_A}\frac{3\beta_{12}+\beta_{345}}{\beta_{245}}, \tag{6}$$

Δ_0^A and Δ_0^B are the maximum energy gap of *A* phase and *B* phase, respectively. β_i is the coefficient of GL expansion and $\beta_{12}=\beta_1+\beta_2$, etc. Using the value of β_i (Ref. 13) and the susceptibility of bulk liquid $\Delta f_A/\Delta f_B$ is about 0.3 at $T=0.8T_c$ and 0.4 at $T=0.9T_c$. In our experimental result this ratio is about 0.3, which is consistent with the above rough estimation at the *A-B* transition. It should be noted that the spatial profile of the order parameter in the slab space is needed to discuss the frequency shift more quantitatively.

C. Supercooling and phase diagram

We observed the interesting phenomena at 10 bar with 2.5 layers of ^{4}H as shown in Fig. 12. At the first, we performed cw NMR measurement on warming up process until above the superfluid transition temperature T_c, whose data is marked with a open circle. We can see a jump of frequency shift which corresponds to the *A-B* transition at $T=0.875T_c$. In the next experiment, we took data in warming up and observed the *A-B* transition again. But before exceeding T_c we began to cool the liquid and took data again, which is marked with solid triangles. From Fig. 12, we can recognize that the resonance frequency obtained on cooling down process continuously shifts toward the high frequency side without any jump in contrast to the temperature dependence on warming up process, where the frequency jump occurred. The *A-B* transition is known as the first order phase transition so our observation is attributed to the supercooling of *A* phase. This metastable state was so stable that we kept observing the supercooling *A* phase until we warmed the liquid again up to $T=0.87T_c$ after cooling down to $T=0.795T_c$. The supercooling *A* phase existed for four days in this run, which is probably due to the smooth surface of polyethylene film, but this is much shorter than the expectation of a life time of metastable *A* phase using a formula of Schiffer *et al.*[34] at $T=0.79T_c$.

On the other hand, all other measurements were taken from the lowest temperature around $T=0.3T_c$ and we always observed the *B* phase signal at the beginning of measurements. The reason of this is as follows. After demagnetizing the nuclear stage we had to wait for one or two days before taking data since our magnet for demagnetization needed time to stabilize its magnetic flux. During this waiting time the *A-B* transition in 1.1 μm cell might occur since the life time of metastable *A* phase at the lowest temperature would be less than an hour.[34]

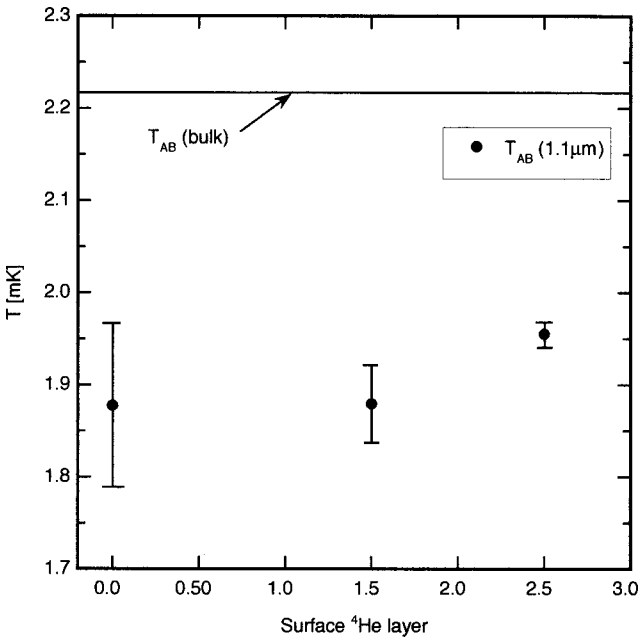

FIG. 14. The effects of surface ^{4}He coverage on $T_{AB}(1.1\,\mu\mathrm{m})$ at 24 bar. The solid line indicates the bulk *A-B* transition temperature.

For pure liquid ^{3}He we plot our measured transition temperature $T_{AB}(1.1\,\mu\mathrm{m})$ on the bulk liquid phase diagram in Fig. 13 with the previous experimental results of Ahonen *et al.*[23] for 4 μm slab spacing, and the theoretical prediction of Li and Ho[13] for 0.5-μm slab geometry with the diffusive surface condition for comparison. It is clear that $T_{AB}(1.1\,\mu\mathrm{m})$ is lower than the bulk liquid T_{AB} (bulk) and at 10 bar it is considerably lower than the predicted *A-B* transition temperature for 0.5-μm slab geometry. We can calculate the critical thickness δ_c defined by a spacing divided by a coherence length at the temperature $T_{AB}(1.1\,\mu\mathrm{m})$, where the shortest coherence length is used, that is $\xi(T)=\xi_T$ with Eq. (2) using the thermodynamic parameter given by Greywall.[27] Our results of critical thickness are 19.8, 30.5, 40.7, and 49.8 at 10, 20, 24, and 27 bar, respectively. These are larger than the expected value of 7.7 in the weak coupling approximation[11] and also larger than those in considering the strong coupling effect, about 10 at 0 bar and about 20 at 20 bar, which depends on the paramagnon parameter.[10] Provided that obtained critical thickness is valid even in 300 nm spacing, we can estimate the coherence length where the *A-B* phase transition should occur in 300 nm and find that these are 15.1 and 9.8 nm at 10 and 20 bar, respectively. These coherence lengths are shorter than the zero temperature coherence length $\xi(0)$ at each pressure; 20 nm and 13.5 nm; respectively. From this speculation we can imagine that the observed phenomena by Freeman *et al.* is not the supercooling but the superfluid state in 300 nm space may not have the *A-B* transition.

Next, we show the effect of surface ^{4}He coverage for $T_{AB}(1.1\,\mu\mathrm{m})$ at 24 bar in Fig. 14. The transition temperature seems to shift to the higher temperature with increasing the surface adsorbed ^{4}He, which is similar to the result by Kawae *et al.*[24] This result, however, is opposite to the theoretical prediction which shows the expansion of *A* phase region when the specular surface condition is achieved. The pressure of 24 bar is high enough to reduce the effect of the superfluidity of ^{4}He film on the ^{3}He quasiparticle scattering.[19–21] So we think that the adsorbed ^{3}He atoms in pure ^{3}He liquid may make the *A* phase stable in this spacing, on the contrary, the surface ^{4}He may make the *B* phase stable. A similar conclusion was reached in a paper by Sprague *et al.*[35] on superfluid ^{3}He in aerogel where the *B* phase appears with adding ^{4}He atoms. But further experiments are needed to settle this problem.

IV. CONCLUSION

We investigated the superfluid ^{3}He in 1.1-μm slab geometry which has a very uniform spacing between parallel plates. We observed the *A-B* phase transition in the superfluid state in this restricted space at 10, 20, 24, and 27 bar. The *A-B* phase transition temperature $T_{AB}(1.1\,\mu\mathrm{m})$ is suppressed by about 15% from T_{AB} (bulk) at higher pressures. This suppression is consistent with the speculation on the anisotropy of the order parameter in the superfluid phase in thin films. The calculated critical thickness δ_c is larger than the expected one but the pressure dependence of our δ_c is consistent with the expectation qualitatively. We need the further experiment in the narrower space to study the spatial variation of the order parameter and the stability of superfluid phase and the effect of boundary condition on them.

ACKNOWLEDGMENTS

We wish to thank Professor K. Nagai gratefully for discussing our study. This work was partly supported by a Grant-in Aid for scientific research from the Ministry of Education, Science and Culture, Japan.

*Present address: President of Osaka City University, Osaka City University, Osaka 558-8585, Japan.

[1] P. W. Anderson and W. F. Morel, Phys. Rev. **123**, 1911 (1961).
[2] R. Balian and N. R. Werthamer, Phys. Rev. **131**, 1553 (1963).
[3] V. L. Ginzburg and L. D. Landau, Zh. Eksp. Teor. Fiz. **20**, 1064 (1950).
[4] L. P. Gorkov, Zh. Eksp. Teor. Fiz. **36**, 1918 (1959).
[5] N. D. Mermin and G. Stare, Phys. Rev. Lett. **30**, 1135 (1973).
[6] V. Ambegaokar, P. G. de Gennes, and D. Rainer, Phys. Rev. A **9**, 2676 (1974); **12**, 345 (1975).
[7] G. Barton and M. A. Moore, J. Low Temp. Phys. **21**, 489 (1975).
[8] I. A. Privorotskii, Phys. Rev. B **12**, 4825 (1975).
[9] L. H. Kjädman, J. Kurkijävi, and D. Rainer, J. Low Temp. Phys. **33**, 577 (1978).
[10] T. Fujita, M. Nakahara, T. Ohmi, and T. Tsuneto, Prog. Theor. Phys. **64**, 396 (1980).
[11] J. Hara and K. Nagai, J. Low Temp. Phys. **72**, 407 (1988).
[12] A. L. Fetter and S. Ullah, J. Low Temp. Phys. **70**, 515 (1988).
[13] Y.-H. Li and T.-L. Ho, Phys. Rev. B **38**, 2362 (1988).
[14] M. T. Manninen and J. P. Pekola, Phys. Rev. Lett. **48**, 812 (1982).
[15] J. P. Pekola, J. C. Davis, and R. E. Packard, Jpn. J. Appl. Phys., Suppl. **26-3**, 113 (1987).

[16] J. G. Daunt, R. F. Harris-Lowe, J. P. Harrison, A. Sachrajda, S. Steel, R. R. Turkington, and P. Zawadski, J. Low Temp. Phys. **70**, 547 (1988).
[17] J. C. Davis, A. Amar, J. P. Pekola, and R. E. Packard, Phys. Rev. Lett. **60**, 302 (1988).
[18] K. Ichikawa, S. Yamasaki, H. Akimoto, T. Kodama, T. Shigi, and H. Kojima, Phys. Rev. Lett. **58**, 1949 (1987).
[19] D. Kim, M. Nakagawa, O. Ishikawa, T. Hata, T. Kodama, and H. Kojima, Phys. Rev. Lett. **71**, 1581 (1993).
[20] S. M. Tholen and J. M. Parpia, Phys. Rev. Lett. **67**, 334 (1991).
[21] A. Matsubara, K. Kawasaki, H. Inaba, S. Miyawaki, O. Ishikawa, T. Hata, and T. Kodama, J. Low Temp. Phys. **114**, 843 (1999).
[22] M. R. Freeman and R. C. Richardson, Phys. Rev. B **41**, 11 011 (1990).
[23] A. I. Ahonen, M. Krusius, and M. A. Paalanen, J. Low Temp. Phys. **25**, 421 (1976).
[24] T. Kawae, M. Kubota, Y. Ishimoto, S. Miyawaki, O. Ishikawa, T. Hata, and T. Kodama, J. Low Temp. Phys. **111**, 917 (1998).
[25] TORAY Industries, Inc.
[26] Mitsubishi Kasei Corporation.
[27] Dennis S. Greywall, Phys. Rev. B **33**, 7520 (1986).
[28] W. F. Brinkman, H. Smith, D. D. Osheroff, and E. I. Blount, Phys. Rev. Lett. **33**, 624 (1974).
[29] O. Ishikawa, Y. Sasaki, T. Mizusaki, A. Hirai, and M. Tsubota, J. Low Temp. Phys. **75**, 35 (1989).
[30] L. R. Corruccini and D. D. Osheroff, Phys. Rev. B **17**, 126 (1978).
[31] H. Ikegami, K. Obara, D. Ito, and H. Ishimoto, Phys. Rev. Lett. **81**, 2478 (1998).
[32] P. Schiffer, M. T. O'Keefe, and D. D. Osheroff, Phys. Rev. Lett. **71**, 1403 (1993).
[33] M. R. Freeman, R. S. Germain, E. V. Thuneberg, and R. C. Richardson, Phys. Rev. Lett. **60**, 596 (1988).
[34] P. Schiffer, M. T. O'Keefe, M. D. Hildreth, Hiroshi Fukuyama, and D. D. Osheroff, Phys. Rev. Lett. **69**, 120 (1992).
[35] D. T. Sprague, T. M. Haard, J. B. Kycia, M. R. Rand, Y. Lee, P. J. Hamot, and W. P. Halperin, Phys. Rev. Lett. **77**, 4568 (1996).